Available online at www.sciencedirect.com

jmr&t Journal of Materials Research and Technology

www.jmrt.com.br

Original Article

Grain refinement mechanism of soft-magnetic alloys with nanocrystals embedded in amorphous matrix

Tao Liu[a,b,c], *Hua Zhang*[a,c], *Fengyu Kong*[d,e,*], *Anding Wang*[d,*], *Yaqiang Dong*[b], *Aina He*[b,*], *Xinmin Wang*[b], *Hongwei Ni*[a,c], *Yong Yang*[d]

[a] *The State Key Laboratory of Refractories and Metallurgy, Wuhan University of Science and Technology, Wuhan 430081, China*

[b] *Key Laboratory of Magnetic Materials and Devices, Ningbo Institute of Materials Technology and Engineering, Chinese Academy of Sciences, Ningbo 315201, China*

[c] *Key Laboratory for Ferrous Metallurgy and Resources Utilization of Ministry of Education, Wuhan University of Science and Technology, Wuhan 430081, China*

[d] *Department of Materials Science and Engineering, College of Engineering, City University of Hong Kong, Kowloon Tong, Kowloon, Hong Kong SAR, China*

[e] *School of Materials and Chemical Engineering, Ningbo University of Technology, Ningbo 315016, Chin0061*

ARTICLE INFO

Article history:
Received 5 December 2019
Accepted 25 January 2020
Available online 19 February 2020

Keywords:
Soft-magnetic alloy
Nanostructure
Grain refinement
Thermal stability

ABSTRACT

To obtain uniform and stable nanostructure with fine α-Fe grains is very important for the wide applications of Fe-based nanocrystalline soft-magnetic alloys. In this study, the nanostructure evolution of the $Fe_{84.75}Si_2B_9P_3C_{0.5}Cu_{0.75}$ (at.%) alloy after annealing under different conditions was characterized in detail. It is found that the alloy exhibits excellent structural stability, which can maintain small α-Fe grains for a prolonged annealing time at low temperature. The increase of annealing temperature and/or annealing time will lead to the precipitation of compound phases in the intergranular amorphous interphase, which affects the α-Fe grains size greatly and determines the structural stability. The elemental mappings of the nanostructured alloys reveal that metalloid elements are enriched in the intergranular amorphous interphase, wrapping around α-Fe grains. The grain refinement and nanostructure stability of these alloys are derived from the shielding and soft-impingement effects of the core-shell like structure. The nanostructure stability is lost with the precipitation of compound phases in the intergranular amorphous interphase, owing to the break-down of the shielding layer, which results in the rapid coarsening of α-Fe grains by coalescence.

* *Corresponding authors*:
E-mails: kongfy@issp.ac.cn (F. Kong), andiwang@cityu.edu.hk (A. Wang), hean@nimte.ac.cn (A. He).

https://doi.org/10.1016/j.jmrt.2020.01.093

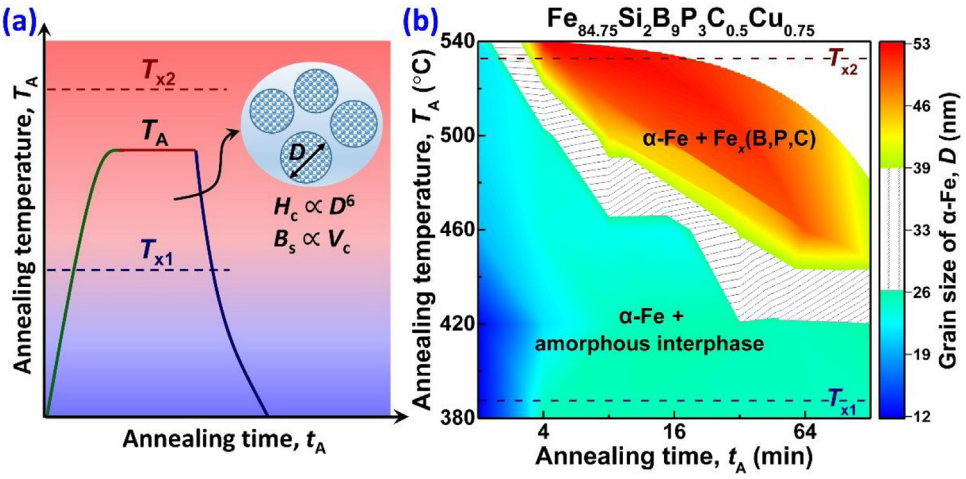

Fig. 1 – (a) Illustration of the annealing temperature window for the nanocrystalline soft-magnetic alloys; Inset sketches the nanocrystalline-amorphous embedded nanostructure; (b) The identified precipitation phases and calculated grains size (D) according to the XRD patterns of $Fe_{84.75}Si_2B_9P_3C_{0.5}Cu_{0.75}$ (at.%) alloy after annealing under different conditions.

1. Introduction

Soft-magnetic alloys are an important electronic materials, which have been playing a crucial role in power generation, transformation and conversion [1]. Among the soft-magnetic materials, Fe-based nanocrystalline alloys have aroused tremendous interest in both industry and academia since developed [2]. These alloys are structurally characterized by nano-sized α-Fe grains in amorphous matrix and functionally characterized by high saturation magnetization (B_s) with unparalleled magnetic softness [3]. In pursuit of higher B_s, a class of high B_s nanocrystalline alloys (HBNAs) with high Fe content (above 82 at.%) and no large atoms (such as Nb, Zr, Mo etc.) were successfully developed [4–6]. These alloys exhibit both high B_s above 1.80 T and excellent soft-magnetic properties as well as low materials cost [7], which are ideal candidates to be used as core materials in transformers, motors, sensors and electric vehicles, for the long-term targets of stronger, lighter, and higher efficiency devices [8].

For the nanocrystalline soft-magnetic alloys, the key is to control the annealing process [9] such that nano-sized α-Fe grains precipitate in amorphous matrix [3]. The correlation between nanostructure and soft-magnetic properties of Fe-based nanocrystalline alloys has been successfully established in random anisotropy model [10,11], that the uniform distribution of fine α-Fe grains in amorphous matrix is conducive to achieving good magnetic softness. Therefore, to unveil the grain refinement mechanism of Fe-based nanocrystalline alloys is helpful to obtain fine nanostructure and achieve excellent soft-magnetic properties. The grain refinement mechanism of Fe-based nanocrystalline alloys has been extensively investigated. As reported in Finemet-type alloys (FeSiBNbCu), the crystallization process is well accepted that Cu-clusters precipitate prior to α-Fe grains at the early stage of annealing process, which can be served as heterogeneous nucleation sites to promote the formation of α-Fe grains [12]. The large atom Nb will hinder the excessive grain growth of α-Fe grains [13] and enable the excellent thermal stability of nanostructure and soft-magnetic properties. However, the HBNAs often suffer from harsh and stringent annealing process. As reported in FeBCu [14] and FeSiBPCu [15] alloys, high heating rate annealing is essential for obtaining small α-Fe grains and good magnetic softness. And for the FeBCCu [16] and FePCCu [17] alloys, the annealing time should be controlled within 3 min in order to avoid any structural coarsening and property degradation. According to Refs. [15,18], the formation of nanocrystals in HBNAs is a competition driven nanocrystallization process, but this is a phenomenological model based on experimental results. The grain refinement mechanism of nanocrystalline soft-magnetic alloys need to be further investigated, and the nanostructure stabilization mechanism is still not clear yet.

In our previous research [19], we developed the $Fe_{84.75}Si_2B_9P_3C_{0.5}Cu_{0.75}$ (at.%) alloy with excellent magnetic properties, and found that the alloy exhibit good thermal stability. Further in this study, the nanostructure of the developed alloy after annealing at different temperature for different time were characterized in detail, to withdraw a comprehensive nanostructure evolution process and provide technical guidance for the controllable preparation of nanocrystalline soft-magnetic alloys. The thermal analyses and elemental mappings of these nanostructured alloys were then conducted, to unveil the grain refinement mechanism of nanocrystalline soft-magnetic alloys. In addition, the nanostructure of the alloy after precipitation of compound phases in residual amorphous matrix and its effects on the further growth of α-Fe grains were also studied, to clarify the nanostructure stabilization mechanism of Fe-based nanocrystalline alloys. These investigations will provide experimental references and theoretical guidance for the development of HBNAs with enhanced thermal stability, which paves the way for the large-scale production of high performance soft-magnetic alloys.

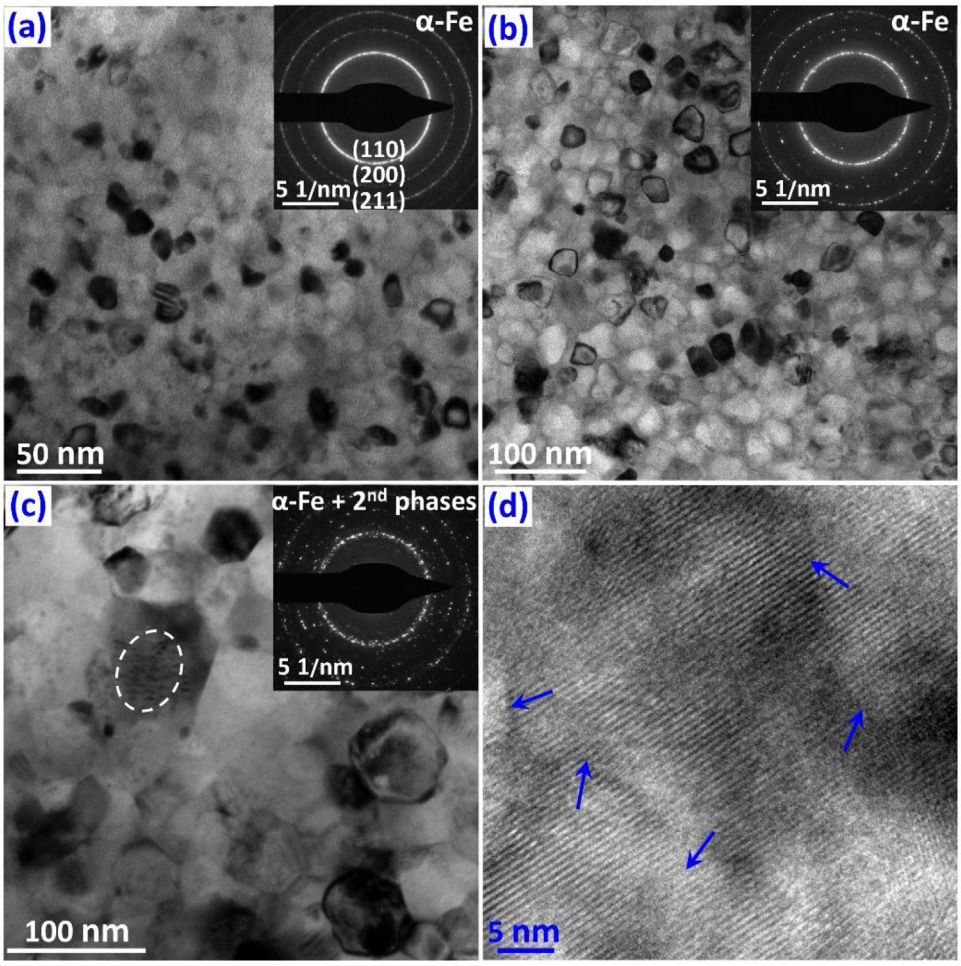

Fig. 2 – TEM bright field images of the $Fe_{84.75}Si_2B_9P_3C_{0.5}Cu_{0.75}$ (at.%) alloy after annealing at 460 °C for (a) 2 min; (b) 16 min; and (c) 64 min, respectively; Inset the corresponding selected area electron diffraction (SAED) patterns; (d) High resolution TEM image of a coarse grain as indicated in Fig. 3(c), and the arrows indicate the boundaries between the sub-grains.

2. Experimental

The master alloy $Fe_{84.75}Si_2B_9P_3C_{0.5}Cu_{0.75}$ (at.%) was prepared by induction melting. Pure elements of Fe (99.99 wt.%), Si (99.99 wt.%), B (99.9 wt.%), Cu (99.99 wt.%), and pre-alloy of Fe_3P and Fe-3.6% C were accurately weighed according to the composition, and melt under an Ar atmosphere after a high vacuum of about 5×10^{-3} Pa. Ribbons about 1 mm wide and 24 μm thick were prepared by using the single-roller melt-spinning method. Isothermal annealing was carried out in a high vacuum tube furnace. The as-quenched ribbon samples were placed in a high vacuum quartz tube and then inserted into a preheated tube furnace to be annealed at different temperature (380–540 °C) for different time (1–120 min) to prepare nanostructured samples. The structure and precipitation phases of the as-quenched and annealed ribbon samples were first identified via X-ray diffraction (XRD, Bruker D8 Advance) with Cu-Kα radiation, and the grain size (D) was calculated according to Scherrer's equation [20,21]. The nanostructure and elemental mappings of the prepared samples were further characterized via high-resolution transmission electron microscopy (TEM, Talos F200), and the TEM samples were prepared via ion milling (Gatan695). Thermal analyses were performed based on the differential scanning calorimetry (DSC, NETZSCH 404C) results of the as-quenched and annealed samples at a heating rate of 40 °C/min.

3. Results

Ribbon samples of the $Fe_{84.75}Si_2B_9P_3C_{0.5}Cu_{0.75}$ (at.%) alloy were readily prepared via induction melting and single-roller melt-spinning techniques. The amorphous structure of the as-quenched ribbons was identified from the XRD results, showing as a broad peak at around 45°. Generally, the amorphous precursors are annealed between the onset crystallization temperature of α-Fe grains (T_{x1}) and 2nd compound phases (T_{x2}) as illustrated in Fig. 1(a). The wide temperature interval between T_{x1} and T_{x2} is beneficial for the formation of nanocrystalline-amorphous embedded nanostructure as sketched in the inset of Fig. 1(a). For the nanocrystalline soft-magnetic alloys, the isothermal annealing temperature (T_A) and annealing time (t_A) both affect the grain size (D) and

volume fraction of α-Fe grains (V_c) greatly. To explore the optimal annealing window is crucial for achieving high B_s [22] and low coercivity (H_c) [3]. Fig. 1(b) shows the precipitation phases and grain size of α-Fe grains obtained from XRD patterns, and T_{x1}, T_{x2} are determined from the DSC curves of the as-quenched ribbon samples. Note that it is quite difficult for the precipitation of α-Fe grains after annealing below 380 °C, and the results are not shown here. The alloys after annealing at a relatively low temperature (380–420 °C) can retain small α-Fe grains for a prolonged annealing time of 120 min. With the increase of annealing temperature (t_A), the stability of α-Fe grains size deteriorates. This is understandable from the perspective of thermodynamics and kinetics of grain growth [23]. Obviously, the further increase of annealing temperature (T_A) or annealing time (t_A) will lead to the precipitation of 2nd phases such as Fe_2B, Fe_3B, Fe_3P, Fe_3C, which results in a sharp increase in α-Fe grain size as shown in Fig. 1(b).

For further structural examination, TEM bright field images of the alloy after annealing at 460 °C for different time were obtained and shown in Fig. 2. After annealing for 2 min, high number density grains with the size of ~18 nm distribute evenly in amorphous matrix as shown in Fig. 2(a). These grains are identified as BCC α-Fe grains from the corresponding selected area electron diffraction (SAED) patterns. After annealing for 16 min, α-Fe grains grow to ~24 nm. The grain size observed in Fig. 2(a and b) is consistent with the calculated results from the XRD patterns in Fig. 1(b). After annealing for 64 min, non-uniform α-Fe grains adjacent to each other can be observed in Fig. 2(c), and the amorphous matrix disappears. The diminishing diffused rings and other diffraction patterns in SAED patterns also indicate the disappearance of intergranular amorphous interphase and the formation of 2nd phases. Note that the coarse grains in Fig. 2(c) are seemingly to be composed of several small sub-grains. This is further confirmed in the high resolution TEM image of a coarse grain as shown in Fig. 2(d). It is clear that the coarse gain contains several small sub-grains, of which the boundaries are marked by the arrows. In other words, the witnessed grain coarsening is due to grain coalescence [24,25].

To understand the crystallization process of the $Fe_{84.75}Si_2B_9P_3C_{0.5}Cu_{0.75}$ (at.%) alloy, DSC was performed on the as-quenched amorphous precursors and nanostructured alloys after annealing at 460 °C for different time. As seen in Fig. 3, two separated exothermic peaks can be easily observed for the as-quenched amorphous ribbons. Based on the results in Fig. 1(b), the first crystallization peak corresponds to the formation of α-Fe grains, and the second one corresponds to the precipitation of 2nd phases such as boride, phosphide and carbide. Thus, with the increase of T_A or t_A, the crystallization process of Fe-based nanocrystalline soft-magnetic alloys can be described as: amorphous → amorphous + α-Fe nano-grains → α-Fe grains + 2nd phases. For the alloy after annealing for 2 min, the first crystallization peak disappears, which suggests a high volume fraction of α-Fe grains (V_c) as observed in Fig. 2(a). This also delivers a strong message that the nucleation and growth of α-Fe grains is ultra-fast for the studied alloys due to the fast diffusion process of HBNAs without large atoms [26]. As the first crystallization peak disappears, the second one shifts to a lower temperature,

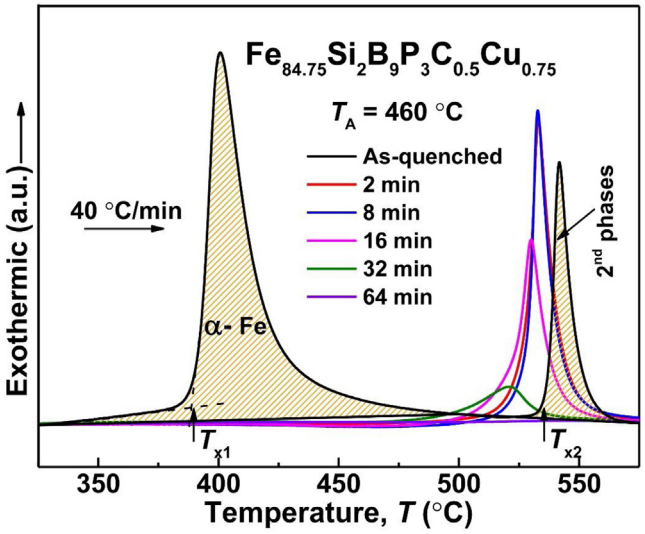

Fig. 3 – DSC curves for the $Fe_{84.75}Si_2B_9P_3C_{0.5}Cu_{0.75}$ (at.%) alloy before and after annealing at 460 °C for different time.

which indicates that the precipitation of α-Fe grains leads to the enrichment of metalloid elements and facilitates the incubation and precipitation of 2nd phases. Notably, the DSC curve of the alloy after annealing for 8 min coincides with the alloy after annealing for 2 min, which means that the changes in nanostructure is negligible for these alloys. With the further increase of t_A, the second crystallization peak shifts to lower temperature and becomes smaller, until disappears after annealing for more than 64 min, indicating the formation of 2nd phases as observed in the inset of Fig. 2(c).

The changes in the second crystallization peak is closely related to the incubation and precipitation processes of 2nd phases, and thereby, elemental mappings of these nanostructured alloy after annealing at 460 °C for different time were then characterized. Since small atoms B and C are unable to be detected, only the high-angle annular dark field (HAADF) images and elemental mappings of P element were shown in Fig. 4. For the alloy after annealing for 2 min, the distribution of P element is relatively uniform, as observed in Fig. 4(d). While for the alloy after annealing for 16 min, P element is obviously enriched around α-Fe grains, as shown in Fig. 4(e), forming a core-shell like structure [27,28], which is the reason for the lower shift of the second crystallization peak as observed in Fig. 3. After annealing for 64 min, phosphorus compound can be easily observed in Fig. 4(f). These phosphides are mainly around α-Fe grains, suggesting that the 2nd phases precipitate in the intergranular amorphous interphase.

4. Discussion

Based on the above experimental findings and analyses, we will first elucidate the formation of nanocrystals in Fe-based nanocrystalline soft-magnetic alloys. During the isothermal annealing process, the samples first keep to its amorphous structure. With the increase of t_A, α-Fe grains begin to precipitate in amorphous matrix, and form a uniform nanostructure with fine α-Fe grains as illustrated in Fig. 5(a). The further

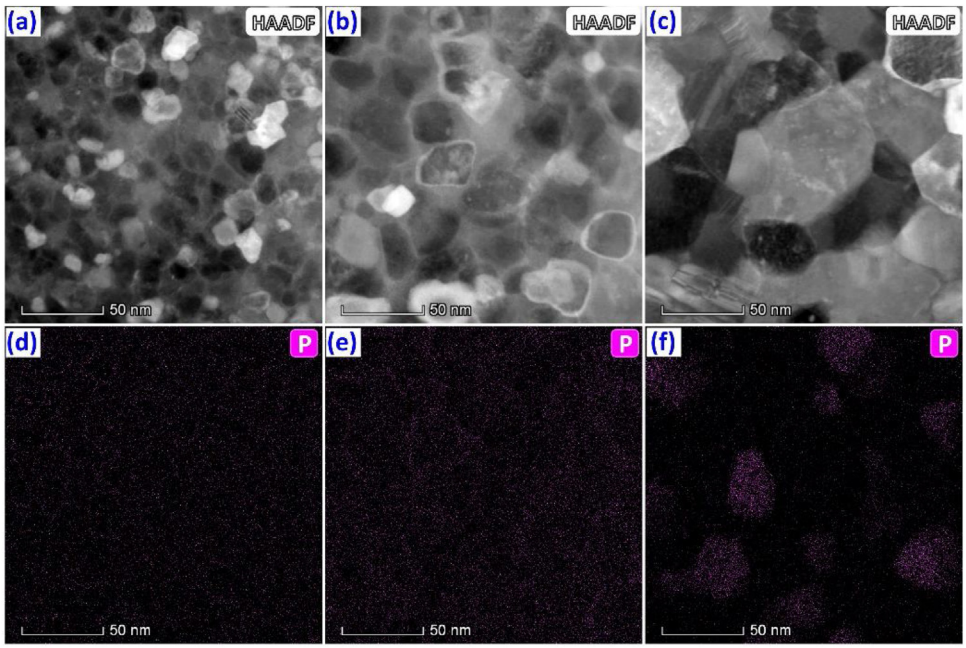

Fig. 4 – High-angle annular dark field (HAADF) images and elemental mappings of P element of the $Fe_{84.75}Si_2B_9P_3C_{0.5}Cu_{0.75}$ (at.%) alloy after annealing at 460 °C for (a) and (d) 2 min; (b) and (e) 16 min; (c) and (f) 64 min, respectively.

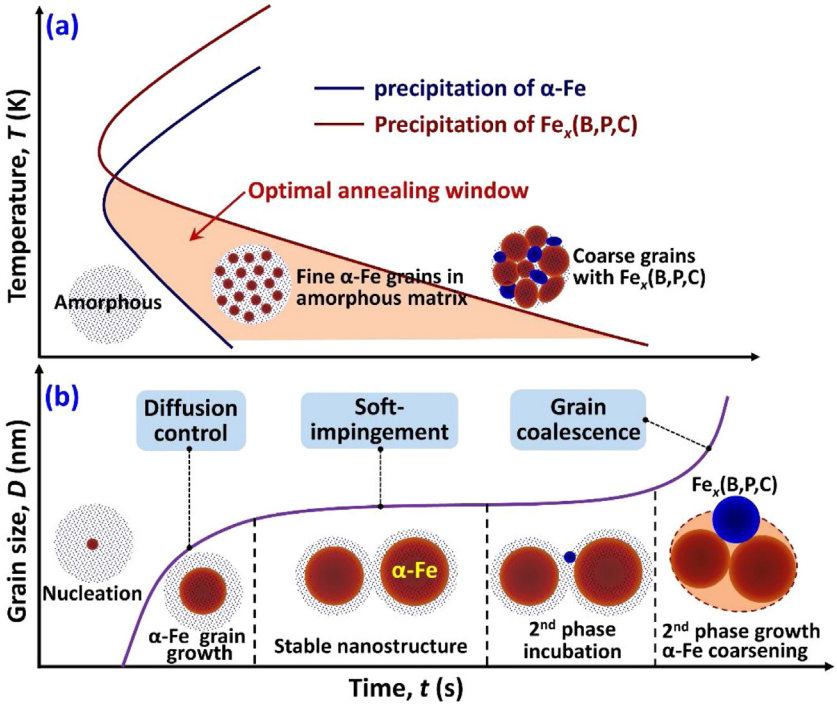

Fig. 5 – Illustrations of (a) formation of nanocrystals during the annealing process; (b) α-Fe grain size changes on the dependence of annealing time; Inset sketches the core-shell like structure evolution during the annealing process.

increase of t_A will lead to the precipitation of 2nd phases and coarsening of α-Fe grains as observed in Fig. 3(c and d). Thus, the optimal annealing window for the Fe-based nanocrystalline soft-magnetic alloys should be within the formation of α-Fe grains and 2nd phases, showing as the shaded area in Fig. 5(a), during which uniform nanostructure with fine α-Fe grains can be obtained. These analyses are quite consistent with the experimental results in Fig. 1(b), that the increase of T_A will narrow the optimal annealing window for obtaining fine α-Fe grains.

Next, we will unveil the grain refinement mechanism and the nanostructure stabilization mechanism of Fe-based

nanocrystalline soft-magnetic alloys. At the early stage of isothermal annealing process, α-Fe grains grow up in a very short time, as observed in Fig. 2(a), owing to the ultra-fast atomic diffusion of HBNAs without large atoms [26]. According to the kinetics of grain growth [29,30], the growth of α-Fe grains can be described as the diffusion of Fe atoms, that α-Fe grains absorb Fe atoms from the surroundings, and creates a Fe-lean inter-layer or interphase wrapping around the α-Fe grains, as observed in Fig. 4(e). The similar results have been extensively reported in HBNAs [31–33], that the metalloid elements are excluded from the α-Fe grains and enriched in the intergranular amorphous interphase, forming a core-shell like structure, which enables the high stability of the alloys [34,35]. The metalloid elements rich (or Fe-lean) layer makes the diffusion of Fe atoms difficult, and thereby hindering the excessive growth of α-Fe grains. In addition, the shielding layer around α-Fe grains will interact with each other, the soft-impingement effect [36,37] between α-Fe grains will also hinder the further growth of α-Fe grains, as sketched in Fig. 5(b). Thus, the grain refinement mechanism of HBNAs stems from the shielding and soft-impingement effects, and the nanostructure stability is closely related to the thermal stability of the shielding layer (or the intergranular amorphous interphase). As observed in Fig. 1(b) and Fig. 4(d), the precipitation of 2nd phases in the intergranular amorphous interphase will lead to the formation of coarse α-Fe grains. This is attributed to the break-down of the shielding layer, which greatly reduces the shielding and soft-impingement effects, resulting in the rapid grain growth by coalescence [24,25], as observed in Fig. 2(c) and Fig. 2(d). For the Finemet-type alloys, the large atoms Nb contributes to a sluggish diffusion process [26] and will also hinder the excessive growth of α-Fe grains [13]. And the good thermal stability of the residual amorphous interphase enables the excellent stability of the nanostructure and properties [38,39].

Finally, we will discuss the implications of this study. The systematic investigations of the formation of nanocrystals in HBNAs will provide technical guidance for the preparation of high performance soft-magnetic alloys by controlling the annealing process. In addition, the revealing of the grain refinement mechanism and nanostructure stabilization mechanism gives us an insight to enhancing the thermal stability of HBNAs. Since the grain refinement and nanostructure stability of Fe-based nanocrystalline alloys stems from the shielding and soft-impingement effects, there are two ways to increase the thermal stability of HBNAs. One is to increase the number density of α-Fe grains to enhance the soft-impingement effects. This has been confirmed in Ref. [40], by increasing the Fe content, the number density of α-Fe grains is greatly increased. As a result, the thermal stability of nanostructure and soft-magnetic properties of HBNAs improves significantly. In that sense, this is similar to the reported competition driven nanocrystallization process [15,18]. The other is to increase the thermal stability of the shielding layer (or the intergranular amorphous interphase). It is reported that the strain energy can act as driving force for ordering [41,42], and which is closely related to the width of the intergranular amorphous interlayer between the grains [43,44]. This can be an effective way to improve the thermal stability of the residual amorphous matrix or prevent the precipitation of 2nd phases in the intergranular amorphous interphase, which is very important for obtaining high performance HBNAs with excellent thermal stability, and warrants further research.

5. Conclusions

In summary, the nanostructured $Fe_{84.75}Si_2B_9P_3C_{0.5}Cu_{0.75}$ (at.%) alloys were obtained via induction melting and melt-spinning techniques, followed by isothermal annealing process. The nanostructure and elemental mappings of the alloys after annealing under different conditions were investigated in detail, to unveil the grain refinement mechanism and nanostructure stabilization mechanism of Fe-based nanocrystalline soft-magnetic alloys. It is found that the alloys after annealing at a relatively low temperature can retain small α-Fe grain size for a prolonged annealing time, and the metalloid elements are enriched around α-Fe grains. The grain refinement and nanostructure stability of HBNAs stems from the shielding and soft-impingement effects. With the further increase of annealing temperature and/or annealing time, 2nd phases will precipitate in the intergranular amorphous interphase, leading to the rapid coarsening of α-Fe grains by coalescence. These results will provide technical guidance for the controllable preparation of high performance HBNAs, and also pave the way for improving the thermal stability of HBNAs, which is of great significance to the large-scale production of high performance soft-magnetic alloys for a variety of industrial applications.

Conflicts of interest

The authors declare no conflicts of interest.

Acknowledgement

This work was supported by the National Key Research and Development Program of China 2016YFB0300501, the National Natural Science Foundation of China Grant No. 51774217, 51601101, 51801224, the Science and Technology Service Network Initiative Grant No. KFJ-STS-SCYD-220, the Zhejiang Provincial Natural Science Foundation Grant No. LQ18E010006, and the Ningbo Municipal Natural Science Foundation Grant No. 2018A610172). YY acknowledges the financial support from Research Grant Council (RGC), the Hong Kong Government, through the general research fund (GRF) with the project numbers CityU11213118 and CityU11200719.

Appendix A. Supplementary data

Supplementary material related to this article can be found, in the online version, at doi:https://doi.org/10.1016/j.jmrt.2020.01.093.

REFERENCES

[1] Silveyra JM, Ferrara E, Huber DL, Monson TC. Soft magnetic materials for a sustainable and electrified world. Science 2018;362(6413), eaao0195.

[2] Yoshizawa Y, Oguma S, Yamauchi K. New Fe-based soft magnetic alloys composed of ultrafine grain structure. J Appl Phys 1988;64(10):6044–6.
[3] Herzer G. Modern soft magnets: amorphous and nanocrystalline materials. Acta Mater 2013;61(3):718–34.
[4] Liu T, Wang AD, Zhao CL, Yue SQ, Wang XM, Liu CT. Compositional design and crystallization mechanism of high B_s nanocrystalline alloys. Mater Res Bull 2019;112:323–30.
[5] Ohta M, Yoshizawa Y. Magnetic properties of nanocrystalline $Fe_{82.65}Cu_{1.35}Si_xB_{16-x}$alloys (x = 0-7). Appl Phys Lett 2007;91(6), 062517-3.
[6] Makino A, Men H, Kubota T, Yubuta K, Inoue A. New Fe-metalloids based nanocrystalline alloys with high B_s of 1.9 T and excellent magnetic softness. J Appl Phys 2009;105(7):07A308.
[7] Xie L, Liu T, He AN, Li Q, Gao ZK, Wang AD, et al. High B_s Fe-based nanocrystalline alloy with high impurity tolerance. J Mater Sci 2018;53(2):1437–46.
[8] Gutfleisch O, Willard MA, Brück E, Chen CH, Sankar SG, Liu JP. Magnetic materials and devices for the 21st century: stronger, lighter, and more energy efficient. Adv Mater 2011;23(7):821–42.
[9] Lu K. Synthesis of nanocrystalline materials from amorphous solids. Adv Mater 1999;11(13):1127–8.
[10] Herzer G. Nanocrystalline soft magnetic alloys. Handbook of magnetic materials 1997;10:415–62.
[11] Bitoh T, Makino A, Inoue A, Masumoto T. Random anisotropy model for nanocrystalline soft magnetic alloys with grain-size distribution. Mater Trans 2003;44(10): 2011–9.
[12] Pradeep KG, Herzer G, Choi P, Raabe D. Atom probe tomography study of ultrahigh nanocrystallization rates in FeSiNbBCu soft magnetic amorphous alloys on rapid annealing. Acta Mater 2014;68:295–309.
[13] Hono K, Ping DH, Ohnuma M, Onodera H. Cu clustering and Si partitioning in the early crystallization stage of an $Fe73.5Si_{13.5}B_9Nb_3Cu_1$ amorphous alloy. Acta Mater 1999;47(3):997–1006.
[14] Zang B, Parsons R, Onodera K, Kishimoto H, Kato A, Liu ACY. Effect of heating rate during primary crystallization on soft magnetic properties of melt-spun Fe-B alloys. Scripta Mater 2017;132:68–72.
[15] Sharma P, Zhang X, Zhang Y, Makino A. Competition driven nanocrystallization in high B_s and low core loss FeSiBPCu soft magnetic alloys. Scripta Mater 2015;95(0):3–6.
[16] Fan XD, Men H, Ma AB, Shen BL. Soft magnetic properties in $Fe_{84-x}B_{10}C_6Cu_x$ nanocrystalline alloys. J Magn Magn Mater 2013;326(0):22–7.
[17] Xiang R, Zhou SX, Dong BS, Zhang GQ, Li ZZ, Wang YG. The excellent soft magnetic properties and corrosion behaviour of nanocrystalline FePCCu alloys. J Mater Sci-mater El 2014;25(7):2979–84.
[18] Li YH, Jia XJ, Xu YQ, Chang CT, Xie GQ, Zhang W. Soft magnetic FeSiBCu nanocrystalline alloys with high Cu concentrations. J Alloys Compd 2017;722:859–63.
[19] Liu T, Kong FY, Xie L, Wang AD, Chang CT, Wang XM, et al. Fe(Co)SiBPCCu nanocrystalline alloys with high B_s above 1.83 T. J Magn Magn Mater 2017;441:174–9.
[20] Patterson AL. The scherrer formula for X-ray particle size determination. Phys Rev 1939;56(10):978–82.
[21] Vorokh A. Scherrer formula: estimation of error in determining small nanoparticle size. Nanosyst Phys Chem Math 2018;9(3):364–9.
[22] Ohta M, Yoshizawa Y. Cu addition effect on soft magnetic properties in FeSiB alloy system. J Appl Phys 2008;103(7):07E722.
[23] Christian JW. The theory of transformations in metals and alloys. Newnes; 2002.
[24] Choi K, Choi JY, Kim DY, Hwang NM. Effect of coalescence on the grain coarsening during liquid-phase sintering of TaC–TiC–Ni cermets. Acta Mater 2000;48(12):3125–9.
[25] Li JJ, Chen JC, Wang H, Chen N, Wang ZC, Guo L, et al. In situ atomic-scale study of particle-mediated nucleation and growth in amorphous bismuth to nanocrystal phase transformation. Adv Sci 2018;5(6):1700992.
[26] Köster U, Herold U, Hillenbrand HG, Denis J. Diffusion in some iron-based metallic glasses. J Mater Sci 1980;15(8):2125–8.
[27] Wu Y, Wang H, Tu WG, Liu Y, Tan YZ, Yuan XZ, et al. Quasi-polymeric construction of stable perovskite-type $LaFeO_3$/g-C_3N_4 heterostructured photocatalyst for improved Z-scheme photocatalytic activity via solid pn heterojunction interfacial effect. J Hazard Mater 2018;347:412–22.
[28] Tahir MB, Asiri AM, Nabi G, Rafiquea M, Sagird M. Fabrication of heterogeneous photocatalysts for insight role of carbon nanofibre in hierarchical WO_3/$MoSe_2$ composite for enhanced photocatalytic hydrogen generation. Ceram Int 2019;45(5):5547–52.
[29] Kelton KF. A new model for nucleation in bulk metallic glasses. Phil Mag Lett 1998;77(6):337–44.
[30] Kelton KF. Time-dependent nucleation in partitioning transformations. Acta Mater 2000;48(8):1967–80.
[31] Liu T, Li FC, Wang AD, Xie L, He QF, Luan JH, et al. High performance Fe-based nanocrystalline alloys with excellent thermal stability. J Alloys Compd 2019;776:606–13.
[32] Jafari S, Beitollahi A, Yekta BE, Ohkubo T, Budinsky V, Marsilius M, et al. Three-dimensional atom probe analysis and magnetic properties of $Fe_{85}Cu_1Si_2B_8P_4$ melt spun ribbons. J Magn Magn Mater 2016;401: 1123–9.
[33] Jafari S, Beitollahi A, Yekta BE, Ohkubo T, Budinsky V, Marsilius M, et al. Atom probe analysis and magnetic properties of nanocrystalline $Fe_{84.3}Si_4B_8P_3Cu_{0.7}$. J Alloys Compd 2016;674:136–44.
[34] Joo SH, Park JY, Tsung CK, Yamada Y, Yang PD, Somorja GA. Thermally stable Pt/mesoporous silica core-shell nanocatalysts for high-temperature reactions. Nature Mater 2009;8(2):126.
[35] Shahzad K, Tahir MB, Sagir M. Engineering the performance of heterogeneous WO_3/fullerene@Ni3B/$Ni(OH)_2$ photocatalysts for hydrogen generation. Int J Hydrogen Energ 2019;44(39):21738–45.
[36] Clavaguera-Mora MT, Clavaguera N, Crespo D, Pradell T. Crystallisation kinetics and microstructure development in metallic systems. Prog Mater Sci 2002;47(6):559–619.
[37] Rassolov S, Tkatch V, Maslov V, Maksimov V, Svyrydova K, Zhikharev I. Nanocrystallization of Al-based glasses via nucleation and growth under “soft impingement” conditions. Phys Status Solidi c 2010;7(5):1340–3.
[38] Um CY, Johnson F, Simone M, Barrow J, McHenry ME. Effect of crystal fraction on hardness in FINEMET and NANOPERM nanocomposite alloys. J Appl Phys 2005;97(10):10F504.
[39] Gheiratmand T, Hosseini HRM. Finemet nanocrystalline soft magnetic alloy: investigation of glass forming ability, crystallization mechanism, production techniques, magnetic softness and the effect of replacing the main constituents by other elements. J Magn Magn Mater 2016;408:177–92.
[40] Liu T, Wang AD, He AN, Wang XM, Liu CT, Yang Y. Co-optimizing magnetic properties and thermal stability of high B_s nanocrystalline alloys with critical formability. J Magn Magn Mater 2019;487:165310.
[41] Song G, Sun ZQ, Poplawsky JD, Gao YF, Liaw PK. Microstructural evolution of single Ni_2TiAl or hierarchical NiAl/Ni_2TiAl precipitates in Fe-Ni-Al-Cr-Ti ferritic alloys during thermal treatment for elevated-temperature applications. Acta Mater 2017;127:1–16.

[42] Rabkin E, Semenov V, Gust W. Coherency strain energy as a driving force for discontinuous ordering. Scripta Mater 1997;37(3):245–51.
[43] Li FC, Liu T, Wang TY, Wang AD, Wang JG, Yang Y. Understanding yielding and the unusual ductile-brittle-ductile transition in Fe-based amorphous nanocrystalline alloy: a combined micromechanical and thermodynamic study. J Mech Phys Solids 2019;132:103681.
[44] Tang C, Harrowell P. Anomalously slow crystal growth of the glass-forming alloy CuZr. Nature Mater 2013;12(6):507.